Geological Survey of Canada
Open File 9232

MICRO- TO NANO-SCALE ANALYSES FOR UNDERSTANDING GOLD PARAGENESIS IN METAMORPHOSED BANDED IRON FORMATIONS NORTH OF RANKIN INLET, NUNAVUT

T.W. Matterson[1], D.C. Petts[2], D. Regis[2], D.E. Moser[1] and J. Czas[2]

Background and Motivation of Study

- The geology surrounding the Meliadine and Meadowbank gold mines, north of Rankin Inlet, NU (Figure 1) has been mapped extensively, but the area northeast of Meliadine has not been studied in great detail, and there is little known about precious metal deportment and mobility in potential ore-bearing units such as Banded Iron Formation (BIF).
- Here we present our first results analysing precious metal deportment (e.g. Au and Ag) using micro-XRF and LA-ICP-MS in BIF samples collected during GSC-UWO regional mapping (GEM-GeoNorth) east of Meliadine in Summer 2023.
- This information will be useful in determining variations in precious metal mineralization, including metals associated with critical minerals, within this region and developing a stronger understanding of the evolution of BIF.

Figure 1: Image taken from Google Earth of the northern Kivalliq region showing the locations of Rankin Inlet, Meliadine Gold Mine and Meadowbank Gold Mine in yellow. The red square indicates the area in which the BIF samples were collected. 70km scale provided for reference.

Regional Geology

- The field area sits in a complex transition zone of greenschist-amphibolite facies Archean and Paleoproterozoic rocks between the Rae and Hearne cratons, which together make up the Churchill Province[1] (Figure 2).
- The Hearne collided into the Rae during the Snowbird orogeny, which occurred at ~1.92 Ga[2].
- Aeromagnetic data from 2013 (Figure 3) shows signatures of highly magnetic rocks spread across the map in thin lines[3], which represent BIF units (Figure 4).

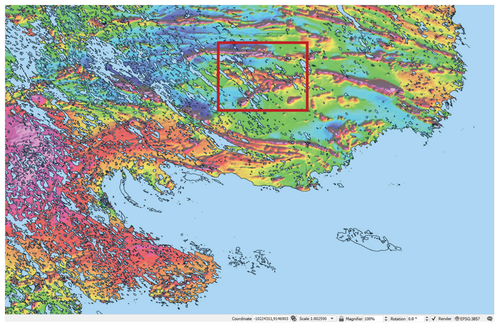

Figure 3: Map showing an aeromagnetic survey of Chesterfield Inlet, NU (Miles and Oneschuk, 2013) with a red box encompassing the field area.

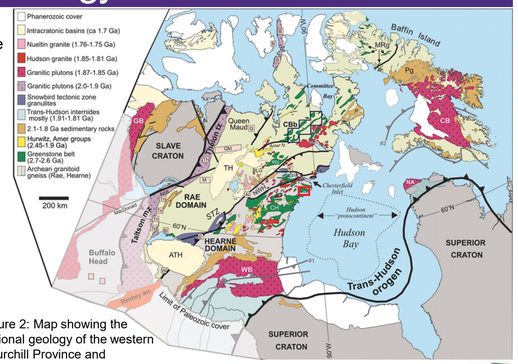

Figure 2: Map showing the regional geology of the western Churchill Province and surrounding areas taken from Berman et al. (2005) indicating the general field area for this study with a red box.

Figure 4: Image taken from one of the BIF localities during fieldwork conducted in July 2023.

Methods

- 11 samples were taken from 9 locations across the BIF (Figure 5).
- Samples were then cut into slabs at the Geological Survey of Canada and then polished at the University of Western Ontario
- 6 of the polished slabs underwent micro-X-ray fluorescence (µXRF) mapping (Figure 6) at the University of Western Ontario to acquire preliminary qualitative element data.
- Laser Ablation Inductively Coupled Plasma Mass Spectrometry (LA-ICP-MS) (Figure 7) was used for all 11 samples to generate quantitative element line profiles (spot size of 80 µm).
- Optical microscopy used for mineralogical and petrologic characterization of the BIF samples.

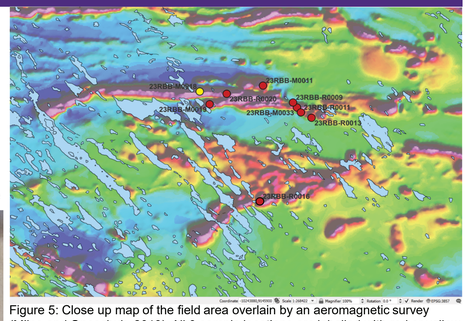

Figure 5: Close up map of the field area overlain by an aeromagnetic survey (Miles and Oneschuk, 2013). All 9 sample locations are labelled with red or yellow dots with the yellow dots indicating the samples that were analyzed for this study (M18A1 and R16F1).

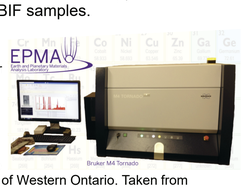

Figure 6: Image of the Bruker M4 Tornado µXRF from the EPMA Lab at the University of Western Ontario. Taken from https://epma.uwo.ca/about/Micro%20XRF.html

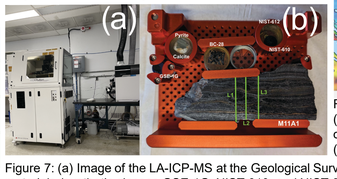

Figure 7: (a) Image of the LA-ICP-MS at the Geological Survey of Canada used for this project. (b) Polished slab (M11A1) and reference materials (synthetic glasses GSE-1G, NIST-610, and NIST-612, magnetite BC-28, as well as in-house pyrite and calcite) mounted for LA-ICP-MS analysis.

Results

- BIF samples were taken from two sections of BIF within the study area, with sample M18A1 coming from the northern section (Figure 5).
- Samples contain alternating layers of magnetite and silicates, with Mn-rich garnets present. As and S tend to correlate with Si, while K concentrations increase within the larger garnet in the top left of sample M18A1 (Figure 8).
- LA-ICP-MS data from M18A1 (Figure 9) shows gold concentrations of up to 38 ppm with the highest concentration of gold being associated with S and As.
  - The highest gold concentrations appear in sample R11A2 with up to 68 ppm gold.
- The highest gold concentrations all occur within the silicate layers, with the highest tending to appear right after a transition from a magnetite or garnet layer into a silicate layer (Figure 9).
- Muscovite, biotite (Figure 10), hornblende, grunerite, garnet, calcite, magnetite, chlorite and quartz have been identified in thin section.
- Garnets are surrounded by calcite in many of the BIF samples (Figure 11).

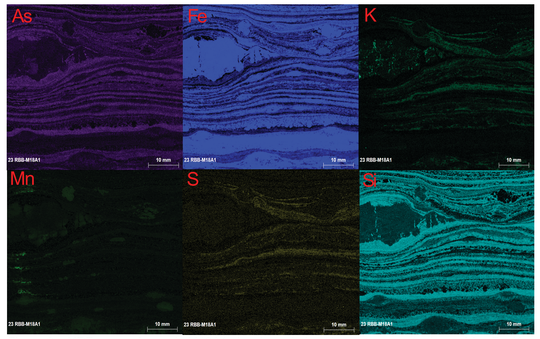

Figure 8: µXRF maps of sample M18A1 showing relative element concentrations of As, Fe, K, Mn, S, and Si. Fe and Si dominant throughout, with As concentrations tending to correlate with Si. Increased Mn concentrations are consistently present within garnets with K appearing in the large garnet in the upper left. 10 mm scale given for all maps.

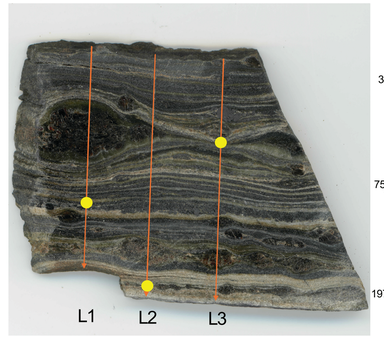

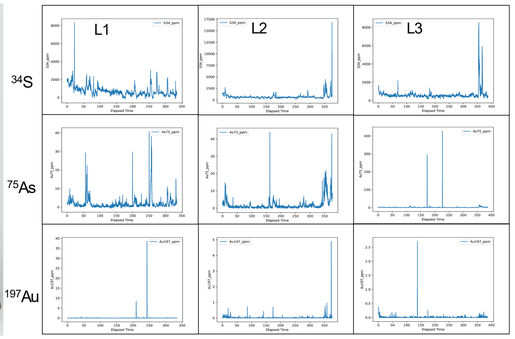

Figure 9: Flatbed scan of sample M18A1 (left) with arrows drawn along the three laser scan lines (L1-L3) to indicate the location of the lines and direction in which the scans were completed. The line scan data (right) shows plots for ^{34}S, ^{75}As, and ^{197}Au, with the highest Au concentrations for each line marked on the flatbed scan with a yellow dot.

Figure 10: Transmitted light XPL photomicrograph of muscovite (ms) and biotite (bt) grains within a silicate layer (qz) of sample M18A1. 100µm scale given for reference.

Figure 11: Photomicrographs of sample M18A1 showing the presence of calcite (cal) surrounding a garnet (gt) and the transition to a silicate layer (qz) below. A transmitted light XPL photomicrograph is shown in (a), while a reflected light photomicrograph is given in (b). 500µm scale given as a reference for both.

Discussions

- There is significant potential for gold mineralization across this BIF layer, as layers with gold concentrations > 2 ppm were identified in all samples (Fig. 9), which at least warrants further investigation into the ore potential of the BIF.
- LA-ICP-MS data was collected with a spot size of 80 µm, so the results only show an average composition of different phases.
- The highest gold concentrations (38 ppm, 68 ppm) are associated with sulfur and arsenic, meaning that they are likely contained within sulfide grains.
- However, this association is not identified for low gold concentrations (< 5 ppm Au), which suggests the presence of free or possibly detrital gold in the BIF.

Conclusions and Future Work

- Preliminary LA-ICP-MS results indicate that we are able to resolve the distribution of precious metals in BIF samples at the micrometre scale.
- Working on large sample surfaces we will build up a library of textures and mineral associations with precious metal occurrences.
- Future work will include Scanning Electron Microscopy-Energy Dispersive Spectroscopy (SEM-EDS) and Electron Backscatter Diffraction (EBSD) analysis, coupled with LA-ICP-MS trace element mapping, to better understand the metal deportment, chemistry, age, and paragenesis of the BIF. Additional thin section petrography will also be carried out.
- We will integrate this information with our parallel regional mapping, structural, and petrochronology analyses of the area east of the Meliadine mine in order to determine mineralization relationships with the regional tectonic evolution.

Acknowledgements

We would like to thank Riccardo Graziani for his support and guidance in the field, and our wildlife monitor, Gordon Anpliarjulc, for guidance on the land. We are also grateful to the GEM-GeoNorth engagement team, in particular Rebecca Pearson and Miranda Adam, for their logistics support, and Aleksandra Mloszewski for internal review of this poster. We also thank Liane Loiselle at the EMPA lab at the University of Western Ontario for providing all the XRF data, as well as Stephen Wood from the Thin Section Lab at the University of Western Ontario for polishing the BIF samples.

References

[1] Berman, R. G., Sanborn-Barrie, M., Stern, R. A., & Carson, C. J. (2005). TECTONOMETAMORPHISM at ca. 2.35 and 1.85 ga in the Rae Domain, Western Churchill Province, Nunavut, Canada: Insights from structural, metamorphic and in situ geochronological analysis of the Southwestern Committee Bay Belt. *The Canadian Mineralogist, 43*(1), 409–442. https://doi.org/10.2113/gscanmin.43.1.409
[2] Corrigan, D., Pehrsson, S., Wodicka, N., & de Kemp, E. (2009). The palaeoproterozoic trans-hudson orogen: A prototype of modern accretionary processes. *Geological Society, London, Special Publications, 327*(1), 457
[3] Miles, W., & Oneschuk, D. (2013). *Chesterfield Inlet, Nu, Aeromagnetic Compilation, Parts of NTS 55 and 65, Nunavut*. https://doi.org/10.4095/292808

[1]Department of Earth Sciences, the University of Western Ontario, 1151 Richmond Street North, London, Ontario N6A 5B7
[2]Natural Resources Canada, Geological Survey of Canada, 601 Booth Street, Ottawa, Ontario K1A 0E8

For more information, please contact D.C. Petts (duane.petts@nrcan-rncan.gc.ca).

OPEN FILE DOSSIER PUBLIC 9232 GEOLOGICAL SURVEY OF CANADA COMMISSION GÉOLOGIQUE DU CANADA 2025

Publications in this series have not been edited; they are released as submitted by the author.

Les publications de cette série ne sont pas révisées; elles sont publiées telles que soumises par l'auteur.

ISSN 2816-7155
ISBN 978-0-660-74990-7
Catalogue No. M183-2/9232E-PDF
https://doi.org/10.4095/pn7ecvcxeg

Recommended citation
Matterson, T.W., Petts, D.C., Regis., D., Moser, D.E., and Czas., J., 2025. Micro- to nano-scale analyses for understanding Au paragenesis in metamorphosed banded iron formations north of Rankin Inlet, Nunavut; Geological Survey of Canada, Open File 9232, 1 poster. https://doi.org/10.4095/pn7ecvcxeg

Natural Resources Canada | Ressources naturelles Canada

2025

Canada